Impact of Architectural Asymmetry on Frank-Kasper Phase Formation in Block Polymer Melts

Alice B. Chang, Frank S. Bates**

Department of Chemical Engineering and Materials Science, University of Minnesota, Minneapolis, MN 55455, United States

ABSTRACT: In recent decades, the discoveries of complex low-symmetry phases in soft matter have inspired advances in molecular and materials design. However, understanding the mechanisms underlying symmetry selection across soft matter remains an important challenge in materials science. Block polymers represent attractive model materials because they permit wide synthetic tunability and provide access to multiple length scales (1–100 nm). However, to date the block polymer design space has been largely limited to variations in molecular weight, block volume fraction, and conformational asymmetry. The molecular architecture – the way in which chains are connected – offers rich potential but remains relatively unexplored in experimental block polymers. Our work bridges this gap, connecting molecular architecture, space-filling demands, and symmetry selection in block polymer self-assembly. Three series of block polymers were synthesized by living polymerization, tuning the architectural asymmetry across the linear-*b*-linear and linear-*b*-bottlebrush limits. The bottlebrush architecture amplifies two key ingredients

for the formation of Frank-Kasper phases: high conformational asymmetry and high self-concentration. Analysis by small-angle X-ray scattering provides insight into the impact of architectural asymmetry on block polymer self-assembly. Increasing the asymmetry between blocks opens the complex phase window, expanding opportunities to tune symmetry selection in block polymer melts.

KEYWORDS: block polymer, self-assembly, Frank-Kasper, quasicrystal, bottlebrush

Self-assembly reflects a multiscale competition between enthalpic and entropic factors, producing periodic nanostructures with rich potential to tune the geometries and length scales. Across all self-assembling soft materials, the shape of the building blocks and penalties associated with elastic deformation play important roles in determining the equilibrium structure.[1-3] Introducing molecular asymmetry can produce a thermodynamic drive to form spherical domains, which resemble soft mesoscopic particles. The formation of these particles occurs in concert with their ordering on a periodic lattice, such that molecular structure, particle size and shape, and lattice symmetry are all intimately connected. In recent decades, the discovery of low-symmetry sphere packings in soft matter has inspired advances across molecular and materials design. The Frank-Kasper lattices, first identified in metal alloys,[4,5] comprise large unit cells with nominally spherical particles of different sizes and shapes in 12-, 14-, 15-, or 16-coordinate environments. Frank-Kasper phases have been identified in a wide variety of soft materials, including dendrons and dendrimers,[6-9] surfactants,[10-14] giant shape amphiphiles,[15-17] and block polymers.[18-27] Despite this profusion of observed low-symmetry phases, understanding the mechanisms underlying symmetry selection across soft matter represents an outstanding challenge in materials science.

Block polymers serve as attractive model materials to address the role of molecular structure in symmetry selection. These compounds afford remarkable synthetic tunability and provide access to multiple self-assembled length scales (1–100 nm). In addition, because block polymers are large, their physics are well-described by coarse-grained statistical theories.[28-30] To date however, in the context of Frank-Kasper phase formation, the block polymer design space has been largely limited to three parameters: block volume fraction, molecular weight,[31] and conformational asymmetry.[23,32] In contrast, other soft systems have experienced wider synthetic manipulations. Structural parameters such as the dendrimer shape,[33,34] surfactant tail length,[35] and vertex substitution in giant shape amphiphiles[16,36] have all been shown to influence symmetry selection. These reports across the soft matter community motivate the need to expand the block polymer design space.

Inspired by dendrimers, surfactants, and giant shape amphiphiles, the way in which block polymer chains are connected – that is, the molecular architecture – emerges as a promising parameter in block polymer design. Recent theory and simulations indicate that the block polymer architecture offers rich potential[37,38] toward the formation of Frank-Kasper phases, but these predictions remain unexplored in experimental systems. In this report, we bridge these gaps by explore the impact of block polymer architecture on the formation of complex low-symmetry phases. Opening the controlled polymerization toolbox permits chains to be connected in many different ways, expanding opportunities for molecular and interfacial shaping.

In order to systematically address the role of architecture, we employed a modular platform for block polymer design based on ring-opening metathesis polymerization (ROMP) (**Fig. 1A**). Functional polynorbornenes permit precise control over the block chemistry, backbone length (N_{bb}), and block volume fraction (f_A). The substituents (R^1 and R^2) can be either discrete or

polymeric, providing access to architectures spanning the linear, comb, and bottlebrush regimes (**Fig. 1B**).[39,40]

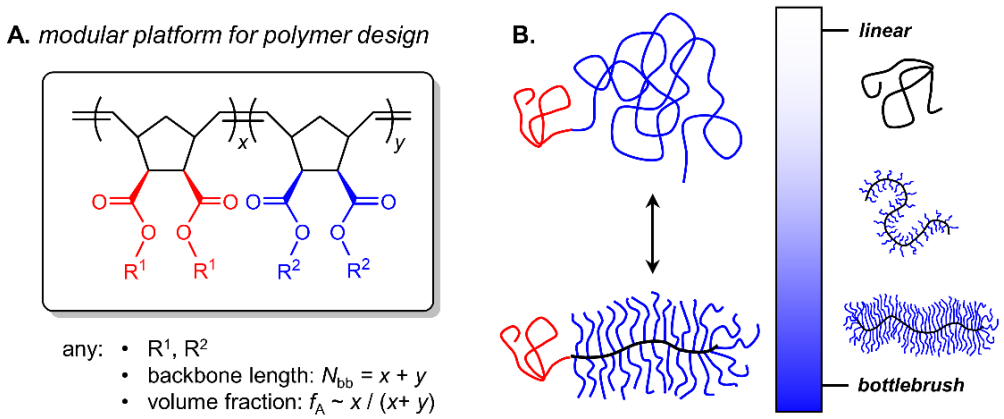

Figure 1. (A) Polynorbornenes provide a modular platform for block polymer design. **(B)** The polymer architecture can be controlled by varying the sizes of the pendant R groups, providing access to linear, comb, and bottlebrush polymers.

The choice of different substituents in the core and coronal blocks (R^1 and R^2, respectively) can produce enormous *architectural asymmetry*. **Figure 1B** illustrates the linear-*b*-linear and linear-*b*-bottlebrush limits. The bottlebrush architecture offers potential to amplify two key ingredients for the formation of Frank-Kasper phases: (1) high conformational asymmetry[23,32] and (2) high self-concentration.[31] Together, these parameters describe how block polymers fill space and ultimately induce symmetry selection.[41] The conformational asymmetry captures the mismatch between the volumes pervaded by each block through the parameter $\varepsilon = (b_A / b_B)^2 \geq 1$, where $b = R_g(6/N)^{1/2}$ is the volume-normalized statistical segment length and R_g is the unperturbed radius of gyration. Self-consistent field theory (SCFT) shows that Frank-Kasper phase formation occurs at $f_A < ½$ when $\varepsilon > 1$, *i.e.* when the block with larger statistical segment length accounts for the minority composition. The self-concentration refers to the ratio of the occupied to pervaded volume, $\phi_s = V_{occupied} / V_{pervaded} \sim \bar{N}^{-0.5}$, where $\bar{N} = Nb^6/v^2$ is the invariant degree of polymerization

and v is the monomer volume. High ε lowers the entropic penalty to stretch A blocks relative to B blocks, while high ϕ_s (equivalently, low $\bar{N}$) increases the geometric frustration associated with packing particles.

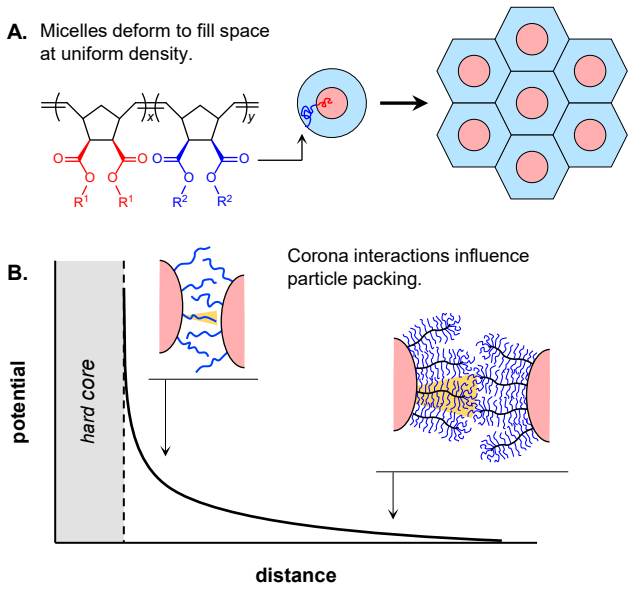

Figure 2. Schematic illustration of the impact of architectural asymmetry on particle packing in diblock polymer melts. **(A)** The block polymers form nominally spherical micelles, which deform in order to fill space at uniform density. **(B)** The soft repulsion between micelles is mediated by the particle coronas. As the distance between micelles decreases, the effective intermicellar potential increases.

Figure 2 provides a schematic illustration of the impact of architectural asymmetry on particle packing in diblock polymer melts. In this scheme (**Fig. 2A**), the minority blocks (*red*) comprise the cores of nominally spherical micelles, and the majority blocks (*blue*) the coronas. *If* these micelles were equally sized hard spheres (like billiard balls), close-packed lattices would maximize the configurational entropy and therefore be the universal equilibrium arrangements.[2] However, block polymer micelles are not simple hard spheres: instead, they are soft particles whose packing depends on both the excluded-volume interactions between hard cores and the entropic repulsion mediated by soft coronas. Decreasing the distance between micelles constrains

the conformations of chains in the corona, thereby decreasing the configurational entropy.[2] As a result, as the distance between micelles decreases, the effective intermicellar potential increases (**Fig. 2B**). In this work, we manipulate the block polymer architecture in order to tune the way in which the coronal chains fill space. Introducing a bottlebrush majority block increases self-concentration (as illustrated by the shaded area in **Fig. 2B**) and ultimately softens the entropic repulsion between particles. The combination of high self-concentration and high conformational asymmetry leads to strong coupling between the shape of the core/corona interface and the shape of the polyhedral Voronoi cell, driving the formation of Frank-Kasper phases.[41]

Complex low-symmetry phases emerge as compromises between the local preference to form spherical domains and the global drive to fill space at uniform density.[20,41] This competition – and the resulting equilibrium geometry – are crucially shaped by the polymer architecture. In this work, we will address the impact of molecular architecture on symmetry selection in diblock polymer melts. **Figure 3** displays three series of polynorbornene diblock polymers synthesized by living ring-opening metathesis polymerization (ROMP). Detailed discussion of the monomer and block polymer syntheses can be found in the Supporting Information (**Schemes S1–S3, Figs. S1–12**). All diblock polymers feature the same core block, poly(norbornene *exo,exo*-dimethylester) (PN2M, R^1 = methyl). The architectural asymmetry was tuned through the steric bulk of the coronal block, which comprises either (**A**) poly(norbornene *exo,exo*-di-*n*-butylester) (PN2B, R^2 = *n*-butyl); (**B**) poly(norbornene *exo*-*n*-decylimide) (PN1D, R^2 = *n*-decyl); or (**C**) poly(norbornene *exo,exo*-di-*n*-decylester) (PN2D, R^2 = *n*-decyl). The side group size increases from Series **A** to Series **B** (*n*-butyl to *n*-decyl), and the number of chains per monomer increases from Series **B** to Series **C** (1 to 2). While PN2M is a linear polymer, recent work suggests that PN2D is a bottlebrush polymer in the asymptotic limit of short side chains but high grafting density.[44,45] As a result,

PN2M-*b*-PN2D represents an architecturally asymmetric linear-*b*-bottlebrush block polymer. Comparisons of Series **A**, **B**, and **C** can therefore be translated into the language of graft and bottlebrush polymers: the *side chain length* increases from **A** to **B**, and the *grafting density* increases from **B** to **C**.

In this work, all diblocks will be specified by the name of the second block (PN2B, PN1D, or PN2D) followed by (f_{PN2M}, N_{bb}), where f_{PN2M} is the volume fraction of the PN2M block and $N_{bb} = x + y$ is the total degree of polymerization of the polynorbornene backbone. The molecular characterization data for all block polymers can be found in **Tables S1** (PN2M-*b*-PN2B), **S2** (PN2M-*b*-PN1D), and **S3** (PN2M-*b*-PN2D). Size-exclusion chromatography (SEC) data indicates that all block polymers are monodisperse ($Đ < 1.1$). Differential scanning calorimetry (DSC) identifies a glass transition temperature for the PN2M block of $T_{g,PN2M} = 32$ °C. The glass transition temperature decreases as the alkyl side chain length increases, *e.g.*, $T_{g,\,PN2D} = -53$ °C (**Figure S13**).

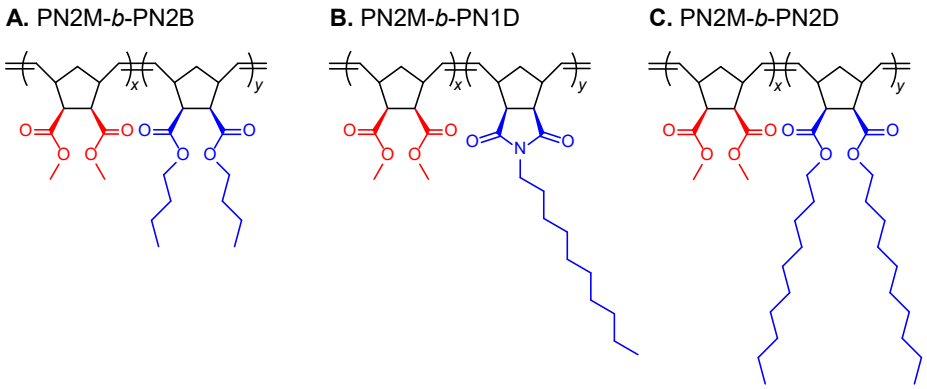

Figure 3. Three series of polynorbornene-based block polymers, each with a poly(norbornene *exo,exo*-dimethylester) (PN2M, R^1 = methyl) minority block (*red*). The steric bulk of the majority block (*blue*) is varied: (**A**) $2R^2$ = *n*-butyl (PN2B), (**B**) $1R^2$ = *n*-decyl (PN1D), (**C**) $2R^2$ = *n*-decyl (PN2D).

RESULTS AND DISCUSSION

Synchrotron-source small-angle X-ray scattering (SAXS) measurements were performed at the Advanced Photon Source at Argonne National Laboratory. The diblock polymers were freeze-dried and hermetically sealed in aluminum pans under argon. For each diblock, one pan was not subject to any thermal treatment; a second pan was annealed at 140 °C for 24 hours, then quenched in liquid nitrogen. At the beamline, SAXS data for both sets of samples (pre-annealed and unannealed) were collected on heating from 25 to 200 °C at 10 °C/min. The phase maps in **Figure 4** display the phases observed for pre-annealed (**A–B**) PN2M-*b*-PN2B and (**C–D**) PN2M-*b*-PN1D block polymers. Each symbol represents a unique diblock with precise composition (f_{PN2M}) and backbone length (N_{bb}). At 25 °C, only the canonical morphologies expected for asymmetric diblock polymers – body-centered cubic spheres (BCC) and hexagonally packed cylinders (HEX_C) – are observed. Upon heating to 190 °C, these samples either retain the low-temperature BCC or HEX_C morphologies or disorder. Assigned morphologies for PN2M-*b*-PN2B and PN2M-*b*-PN1D are summarized in **Tables S4–S5**; 1D-averaged SAXS data on heating from 25 to 200 °C are provided in **Figures S14–S15**.

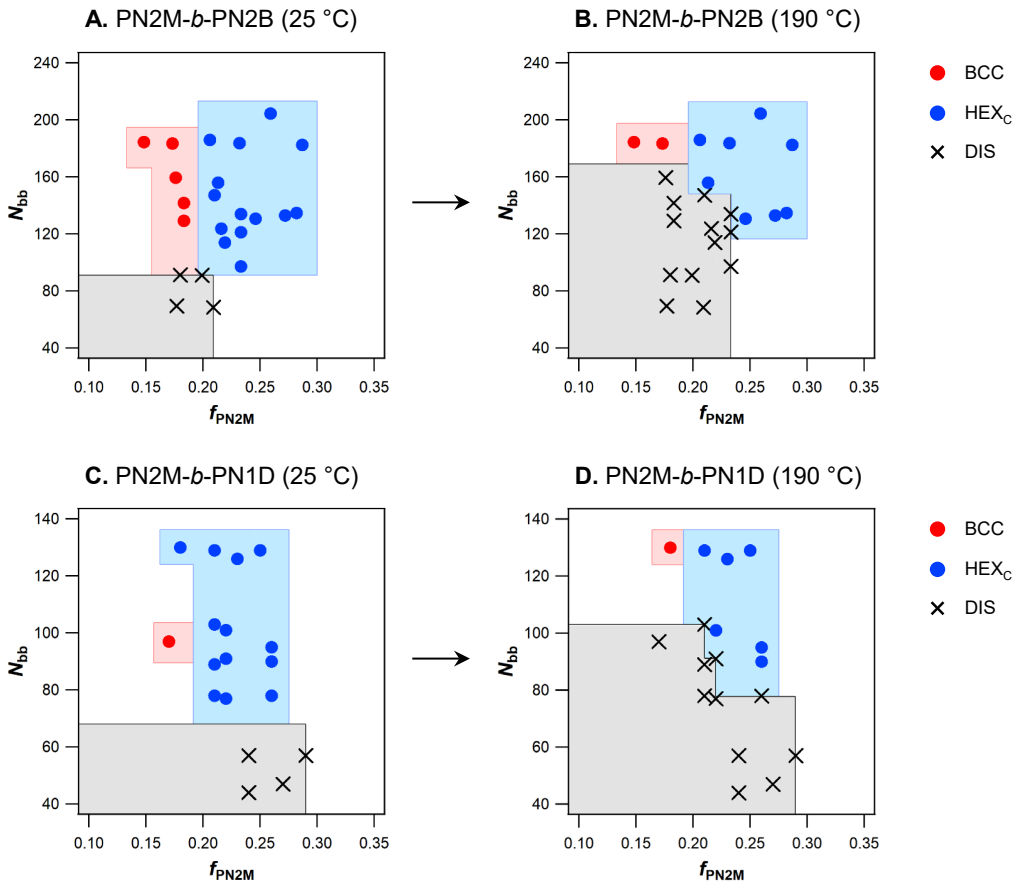

Figure 4. Phase maps for **(A–B)** PN2M-*b*-PN2B and **(C–D)** PN2M-*b*-PN1D determined by synchrotron-source small-angle X-ray scattering (SAXS) at 25 °C and 190 °C. Each symbol represents a unique diblock with precise composition (f_{PN2M}) and backbone length (N_{bb}).

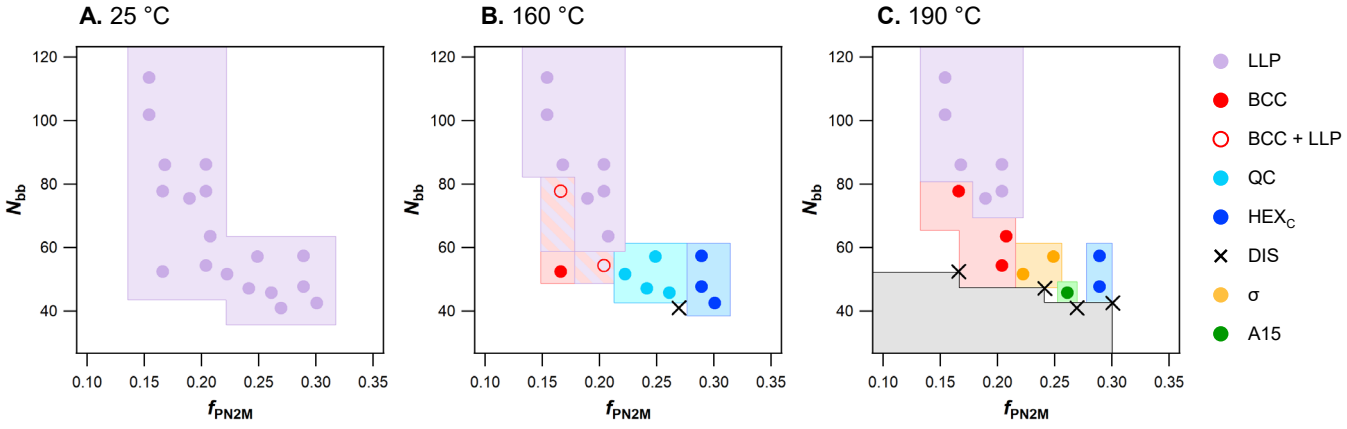

Figure 5. Phase maps for unannealed PN2M-*b*-PN2D block polymers determined by synchrotron-source small-angle X-ray scattering (SAXS) at **(A)** 25 °C, **(B)** 160 ° C, and **(C)** 190 °C. Each symbol represents a unique diblock with precise composition (f_{PN2M}) and backbone length (N_{bb}).

In contrast to the canonical phase behavior observed for PN2M-*b*-PN2B and PN2M-*b*-PN1D (**Fig. 4**), the phase maps for the bulkier PN2M-*b*-PN2D block polymers reveal remarkable complexity. Unannealed PN2M-*b*-PN2D diblocks were heated at 10 °C/min to each target temperature (25, 60, 80, 100, 140, 150, 160, 170, 180, 190, 200 °C) and annealed for 15 minutes at each temperature prior to collecting data. **Figure 5** presents the phases observed at (**A**) 25 °C, (**B**) 160 °C, and (**C**) 190 °C. The rich phase behavior that emerges illustrates the potential of architectural asymmetry to open the complex phase window. At 25 °C (**Fig. 5A**), all diblocks adopt disordered liquid-like packings (LLP) that offer analogies to supercooled liquids and soft glasses.[46,47] Upon heating to 160 °C (**Fig. 5B**), high-molecular-weight diblocks ($N_{bb} > 60$, $M_n > 20$ kDa) remain jammed in the LLP state. In contrast, low-N_{bb} diblocks evolve into different morphologies: as the core volume fraction (f_{PN2M}) increases, samples form (1) body-centered cubic (BCC) spheres, (2) dodecagonal quasicrystals (DDQC), or (3) hexagonally packed cylinders (HEX_C). Dodecagonal quasicrystals feature local twelve-fold symmetry and quasi-periodic order in two dimensions. Whereas BCC, HEX_C, and other phases are periodic in three-dimensional space, dodecagonal quasicrystals can only be considered periodic in higher-dimensional space.[48,49] Both LLP and DDQC suggest local clustering in kinetically arrested, non-equilibrium states, which may seed the growth of complex phases at higher temperatures.[22,24] The connection between LLP and DDQC invokes long-standing mysteries surrounding the origin of symmetry selection in soft materials.

Upon heating to 190 °C (**Fig. 5C**), high-N_{bb} samples remain in LLP states even at long times (>12 hr). However, the low-N_{bb} DDQC-forming samples evolve into well-ordered Frank-Kasper σ ($0.22 \leq f_{PN2M} \leq 0.25$) or A15 ($f_{PN2M} = 0.26$) phases. **Figure 6** displays the 1D-averaged SAXS patterns for three unannealed PN2M-*b*-PN2D diblock polymers on heating from 25 to 200

°C. All three diblocks adopt LLP at 25 °C, but different morphologies evolve upon heating depending on the volume fraction and molecular weight. As f_{PN2M} increases, (**A**) BCC spheres, (**B**) the Frank-Kasper σ phase, or (**C**) the Frank-Kasper A15 phase were observed. For all PN2M-*b*-PN2D diblocks, the assigned morphologies and 1D-averaged SAXS data on heating from 25 to 200 °C are provided in the Supporting Information. Data for samples that were pre-annealed in the same way as PN2M-*b*-PN2B and PN2M-*b*-PN1D are provided in **Table S6** and **Figure S16**; data for samples that were *not* pre-annealed (as summarized in **Figure 5**) are provided in **Table S7** and **Figure S17**. Indexed patterns for the Frank-Kasper σ and A15 phases are provided in **Figures S18** and **S19**, respectively.

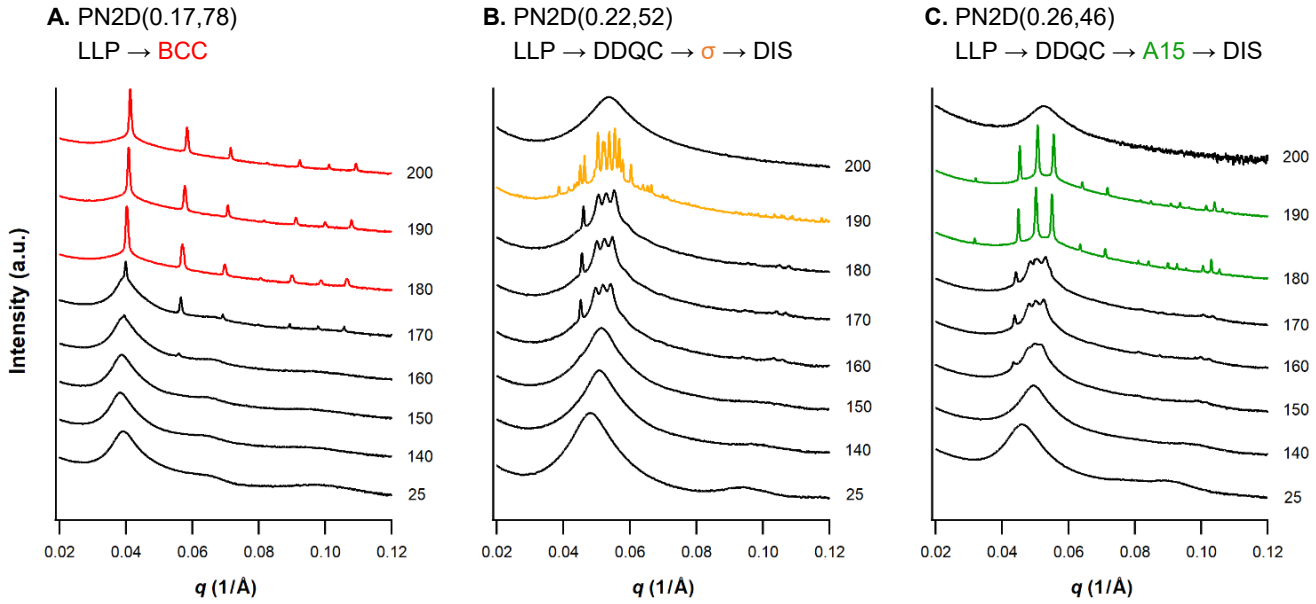

Figure 6. 1D-averaraged SAXS patterns for three unannealed PN2M-*b*-PN2D(f_{PN2M} , N_{bb}) block polymers on heating. All three block polymers adopt liquid-like packings (LLP) at 25 °C. Different morphologies emerge on heating: as the volume fraction (f_{PN2M}) increases, (**A**) body-centered cubic (BCC) spheres, (**B**) the Frank-Kasper σ phase, or the (**C**) Frank-Kasper A15 phase are observed.

The Frank-Kasper σ phase ($P4_2/mnm$) has been experimentally identified in melts of several types of diblock polymers, including poly(1,4-isoprene)-*b*-poly($_{D,L}$-lactide) (PI-*b*-

PLA),[18,20-24] poly(ethylethylene)-*b*-poly($_{D,L}$-lactide) (PEE-*b*-PLA),[23] and poly(dimethylsiloxane)-*b*-poly(2,2,2-trifluoroethyl acrylate) (PDMS-*b*-PTFEA).[25] In comparison, the Frank-Kasper A15 phase ($Pm\bar{3}n$) remains rare in diblock polymer melts. Although it has been observed in a variety of other self-assembled soft materials – including discrete surfactants,[35] molecular tetrahedra,[15] dendrimers,[6,9,50] hydrated oligomers,[12,51,52] and bidisperse diblock polymer blends[53] – the A15 phase has been experimentally identified in only one diblock polymer melt to date: poly(dodecyl acrylate)-*b*-poly($_{D,L}$-lactide) (PDDA-*b*-PLA).[19] In these diblocks, the 12-carbon dodecyl side chains amplify conformational asymmetry [$\varepsilon = (b_{PLA}/b_{PDDA})^2 = 3.4$] and widen the complex phase window. Comparisons of PDDA-*b*-PLA to the polynorbornene diblock polymers introduced in this work are provided in the Discussion section.

In order to provide insight into the formation of A15 in diblock melts, the phase behavior of A15-forming PN2M-*b*-PN2D(0.26,46) was further explored. The evolution of A15 on slow heating is shown in **Figures 6C** and **S17**. From the low-temperature LLP state, quasicrystals emerge at 150 °C and persist up to 170 °C. A15 begins to emerge at 170 °C, becomes pure at 180 °C, and disorders at 200 °C. The direct DDQC → A15 transition is relatively uncommon among self-assembling soft materials; in previous reports, HEX_C → A15[50,51,54] or σ → A15[16,52] transitions are more commonly observed. In order to probe the DDQC → A15 transition, a second unannealed sample of PN2M-*b*-PN2D(0.26,46) was heated from 25 to 170 °C at 10 °C/min, then from 170 to 213 °C at approximately 1.5 °C/min (**Figure 7**). The sample adopts LLP at 25 °C and retained LLP through heating to 170 °C (**A**, 162 °C; **B**, 170 °C). At 170 °C, DDQC emerges (**B**) and persists for 10 minutes (**C**). The quasi-periodic DDQC structure observed in physical space can be described in terms of projections from five-dimensional space, where the DDQC structure is periodic. In order to describe allowed reflections in five dimensions, five linearly independent

vectors are required, corresponding to five-integer generalized Miller indices.[48,49] The four peaks observed in **Fig. 7C** correspond to the characteristic (00002), (12100), (10102), and (12101) reflections for dodecagonal quasicrystals.[21,49,55] Upon slow heating from 170 °C, the Frank-Kasper A15 phase nucleated at 186 °C (**D**), as evidenced by the emergence of characteristic (200), (210), and (211) reflections. The A15 phase became pure at 190 °C (**E**) and began to disorder at 213 °C (**F**).

The SAXS data suggest that the (00002) plane of the DDQC structure, corresponding to the interplanar spacing, becomes the (200) plane of the A15 lattice. Analogous to the reported DDQC-to-σ transition,[21] nucleation and growth of the A15 phase from DDQC likely occurs *via* rearrangement of particles in the quasiperiodic *x*-*y* plane without changing the interplanar spacing in the *z* direction. Previous reports of A15-forming soft materials suggest that slow chain exchange favors the initial formation of DDQC over HEX_C, because quasicrystals more readily accommodate the wide distribution of particle sizes that result from heating the kinetically jammed LLP state.[52,53] The connections between LLP, quasicrystals, and complex phases continue to inspire interest and will be explored in future work.

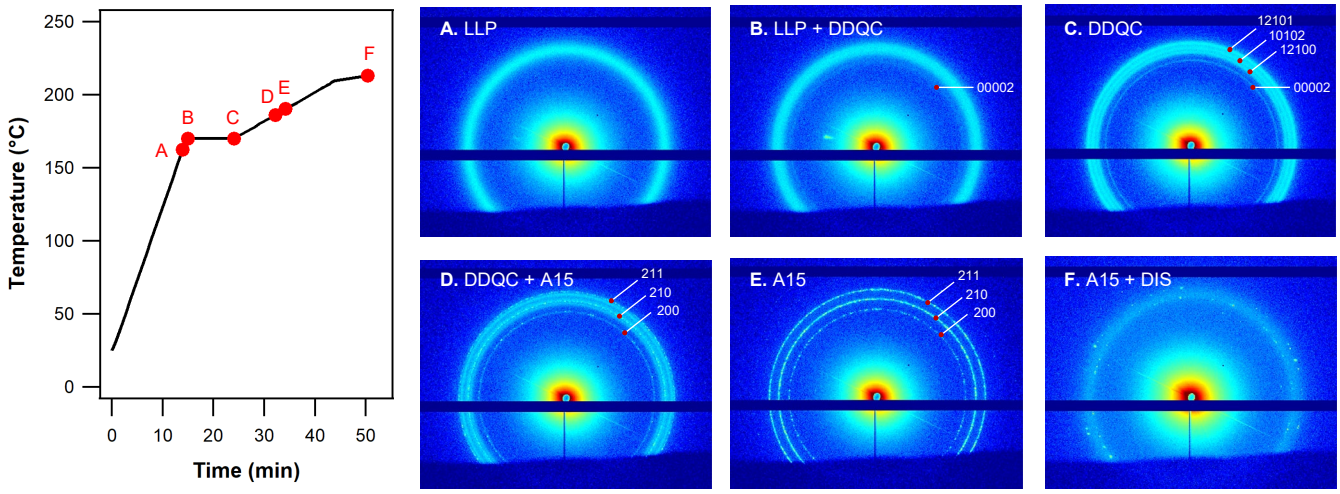

Figure 7. SAXS data on heating PN2D(0.26,46). At 25 °C, the sample adopts liquid-like packing (LLP). The sample was heated to 170 °C at 10 °C/min, then slowly heated to 213 °C at an average rate of 1.5 °C/min. The sample retained LLP through heating to 170 °C (**A**, 162 °C; **B**, 170 °C). At 170 °C, DDQC emerges (**B**) and persists for 10 minutes (**C**). Upon slow heating, the Frank-Kasper A15 phase nucleates at 186 °C (**D**) and becomes pure at 190 °C (**E**). At 213 °C, coexistence between A15 and disorder is observed (**F**).

The materials introduced in this work provide insight into the impact of molecular architecture on symmetry selection in block polymer melts. Three series of asymmetric diblock polymers were synthesized, which all share the same minority block (poly[norbornene *exo,exo*-dimethylester], PN2M) but vary the steric bulk of the second block: (**A**) poly(norbornene *exo,exo*-di-*n*-butylester), PN2B; (**B**) poly(norbornene *exo*-*n*-decylimide), PN1D; or (**C**) poly(norbornene *exo,exo*-di-*n*-decylester), PN2D. As a consequence of compositional asymmetry ($f_{PN2M} < 0.30$), the block polymers form soft particles that order on a periodic lattice. The multiscale competition to minimize both interfacial area and chain stretching can lead to the formation of equilibrium Frank-Kasper σ and A15 phases.[41] These complex low-symmetry phases have been experimentally identified in linear diblock polymers featuring high conformational asymmetry and high self-concentration.[18-24,31] *Non-linear* architectures remain relatively unexplored but offer rich potential to amplify both conformational asymmetry and self-concentration. We will discuss how

architectural variations – represented by (**A**) PN2M-*b*-PN2B, (**B**) PN2M-*b*-PN1D, and (**C**) PN2M-*b*-PN2D – influence the formation of complex low-symmetry phases in block polymer melts.

Recent reports define the comb and bottlebrush regimes in terms of the spacing between grafts along the backbone (L_g) and the side chain size (expressed through the diameter of gyration, $2R_{g,sc}$).[40,43] When $L_g > 2R_{g,sc}$, the backbones behave like flexible Gaussian chains; when $L_g < 2R_{g,sc}$, the backbones stretch, leading to extended, wormlike conformations. The onset of the bottlebrush regime at $L_g = 2R_{g,sc}$ marks a transition to different chain statistics and physical properties compared to linear and comb polymers. In this work, all blocks (PN2M, PN2B, PN1D, and PN2D) feature a polynorbornene main chain. Each norbornene repeat unit has a contour length of 6.2 Å, suggesting that pendant groups with dimensions larger than 6.2 Å may induce sufficient steric crowding to access the bottlebrush regime. We note that this interpretation is consistent with recent reports of bottlebrush poly(α-olefins) with discrete *n*-alkyl side chains (C4–C18).[45,56,57] However, the C4 and C10 groups in this work are not sufficiently large to adopt Gaussian coil conformations, which are assumed by most theoretical treatments of comb and bottlebrush polymers.[39,40,43] In such treatments, the side chain size is typically expressed in terms of the unperturbed diameter of gyration, $2R_{g,sc}$; in this work, as an initial approximation, the side group size will instead be expressed in terms of the *n*-alkyl chain length, l_{sc}. For the reported polynorbornenes,

$$l_{flex} \leq l_{sc} \leq l_{max} \quad (1)$$

where l_{flex} and l_{max} correspond to the typical flexible configuration in the bulk and the maximally extended, all-*trans* configuration, respectively.[58,59] For n carbons in an *n*-alkyl chain,

$$l_{max} = 1.53 + 1.265(n-1) \quad (2)$$

$$l_{flex} = 1.53 + 0.925(n-1) \quad (3)$$

Table 1 provides estimated lengths L_g, l_{flex}, and l_{max} for the coronal blocks PN2B, PN1D, and PN2D. In the language of comb and bottlebrush polymers, the side chain length increases from PN2B (n = 4) to PN1D and PN2D (n = 10); the grafting density z, defined as the number of side chains per backbone repeat unit, doubles from PN1D (z = 1) to PN2B and PN2D (z = 2). The average spacing between grafts is given by $L_g = L_c / z$, where L_c = 6.2 Å is the contour length per norbornene unit. Direct analogy to previous reports – which require bottlebrush polymers to satisfy $L_g \leq 2R_{g,sc}$ – suggests that PN2B, PN1D, and PN2D all resemble bottlebrushes, since $L_g \leq l_{sc}$ according to Eq. 1. We emphasize that this comparison is not exact, since these discrete polynorbornenes represent an asymptotic limit of extremely short side chains and high grafting density in the graft polymer design space. However, recent reports demonstrate that similar treatment of poly(α-olefins) with discrete *n*-alkyl side groups captures key physical properties associated with bottlebrush polymers, such as the increasing entanglement molecular weight[45] and extensibility[57] with increasing n. These analyses identified poly(1-hexene), which has a two-carbon backbone repeat unit and *n*-butyl side groups, as the transition from the comb to bottlebrush regime.[56]

Table 1. Estimated spacing between grafts (L_g) and side chain lengths (l_{flex}, l_{max}).

Polymer	***n***	***z***	L_g **(Å)**	l_{flex} **(Å)**	l_{max} **(Å)**
PN2B	4	2	3.1	4.3	5.3
PN1D	10	1	6.2	9.9	12.9
PN2D	10	2	3.1	9.9	12.9

The crossover from combs to bottlebrushes signals a transition from flexible to extended backbones, and from interpenetrating to non-penetrating side chains. In the bottlebrush limit,

polymers resemble flexible mesoscopic cylinders with high self-concentration. High self-concentration is crucial for the formation of complex low-symmetry phases in block polymer melts: forcing chains to fill space at high self-concentration amplifies elastic penalties and conformational asymmetry, motivating strong coupling of the core/corona interface with the shape of the Voronoi cell.[19,31,41] Quantitative estimates of self-concentration would require an analytical expression for the volume pervaded by the brush, for which no consensus exists to the best of our knowledge. As a proxy for understanding brush interpenetration, we instead consider backbone-backbone distances inferred from mid- and wide-angle X-ray scattering measurements (MAXS/WAXS). **Figure 8A** shows the 1D-averaged MAXS and WAXS data for select unannealed PN2M-*b*-PN2D block polymers at 25 °C. The molecular characterization data and assigned morphologies are provided in **Tables S3** and **S6**, respectively. No evidence of crystallization was observed by either WAXS or differential scanning calorimetry (DSC) (**Figure S13**). Two scattering peaks were observed for each block polymer, regardless of composition ($0.17 \leq f_{PN2M} \leq 0.50$). For PN2M-*b*-PN2D, a low-q peak appears at $q_1 = 0.260 \pm 0.004$ Å^{-1}, and a high-q peak appears at $q_2 = 1.38 \pm 0.01$ Å^{-1}. Previous reports of amorphous bottlebrush polymers with *n*-alkyl side chains have identified similar peaks at low- and high-q.[45,56,60] The low-q feature corresponds to the average distance between backbones ($d_{bb} = 2\pi/q_1$), whereas the high-q feature corresponds to the average distance between *n*-alkyl side chains ($d_{sc} = 2\pi/q_2$) (**Figure 8B**). The distances d_{bb} and d_{sc} for PN2B, PN1D, and PN2B coronal blocks are compiled in **Table 2**; MAXS and WAXS data for PN2M-*b*-PN2B and PN2M-*b*-PN1D block polymers are provided in the Supporting Information (**Figures S20–21**).

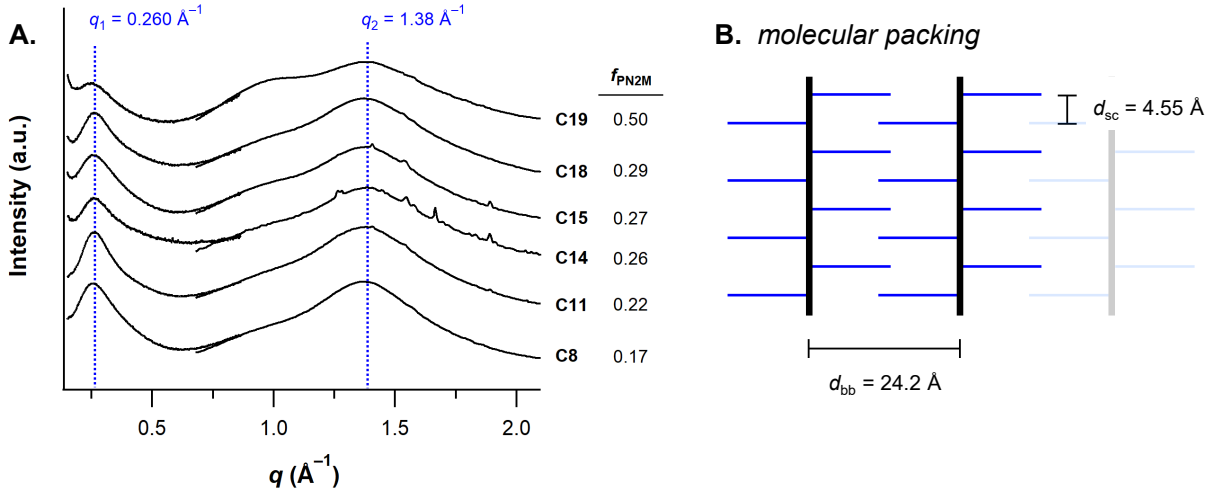

Figure 8. (A) 1D-averaged mid- and wide-angle X-ray scattering (MAXS and WAXS) data for select PN2M-*b*-PN2D block polymers at 25 °C. $q_1 = 0.260 \pm 0.004$ Å^{-1} corresponds to the average distance between backbones, and $q_2 = 1.38 \pm 0.01$ Å^{-1} corresponds to the average distance between *n*-decyl side chains. **(B)** Schematic illustration of average backbone distances ($d_{bb} = 2\pi/q_1$) and side chain distances ($d_{sc} = 2\pi/q_2$) in PN2D. Note that the small sharp peaks in the C14 and C15 traces in (**A**) are artifacts due to stray scattering on the area detector.

Table 2. Average backbone distances (d_{bb}) and side chain distances (d_{sc}), calculated from MAXS and WAXS data. d_{bb}, l_{flex}, and l_{max} values were used to estimate the *n*-alkyl side chain lengths (l_{sc}).

Polymer	d_{bb} (Å)	d_{sc} (Å)	l_{sc} (Å)
PN2B	not obs.	4.65 ± 0.02	4.3–5.3
PN1D	22.9 ± 0.4	4.73 ± 0.01	11.4–12.9
PN2D	24.2 ± 0.4	4.55 ± 0.02	12.1–12.9

No low-q scattering peaks were observed for PN2M-*b*-PN2B, suggesting that the spacing between polynorbornene main chains is not well-defined. In contrast, both PN1D and PN2D have well-defined backbone distances: for PN1D, $d_{bb} = 22.9 \pm 0.4$ Å, and for PN2D, $d_{bb} = 24.2 \pm 0.4$ Å. The side chain lengths l_{sc} can be estimated from d_{bb} and Eq. 1. Schematic illustrations of the two limiting cases for l_{sc} are provided in **Figure S22**. If no intermolecular side chain overlap occurs – that is, at maximum self-concentration – $l_{sc} = d_{bb}/2$; on the other hand, if maximum intermolecular

overlap occurs, $l_{sc} = l_{max}$. These ranges ($d_{bb}/2 \leq l_{sc} \leq l_{max}$) are provided in **Table 2**. The smaller backbone spacing d_{bb} observed for PN1D compared to PN2D suggests that, in PN1D, either the side chains are less extended *or* the extent of side chain interdigitation / intermolecular overlap is greater. Either case suggests that PN1D is less bottlebrush-like than PN2D, as anticipated by its lower grafting density ($z = 1$ for PN1D; $z = 2$ for PN2D). In other words, the PN2D coronal block features the highest self-concentration in this work.

In addition to high self-concentration, high conformational asymmetry is a key ingredient in the formation of complex low-symmetry phases in block polymer melts. Conformational asymmetry captures the mismatch between the volumes pervaded by each block through $\varepsilon = (b_A/b_B)^2 \geq 1$, where b_A and b_B are the statistical segment lengths of the core (A) and coronal (B) blocks. Introducing branching in the corona, either through miktoarm star architectures or bulky side groups,[32] increases ε. For example, several recent reports describe the formation of the Frank-Kasper σ and A15 phases in diblocks with a poly(D,L-lactide) (PLA) core and a branched coronal block.[23,25] Two systems feature a main chain in the coronal block with two-carbon repeats and *n*-alkyl side groups: PLA-*b*-poly(ethylethylene) (PLA-*b*-PEE, $\varepsilon = 1.7$) and PLA-*b*-poly(dodecyl acrylate) (PLA-*b*-PDDA, $\varepsilon = 3.4$). As the side group size increases ($n = 2$ for PEE; $n = 12$ for PDDA), the conformational asymmetry increases. The same trend occurs for the polynorbornene-based block polymers introduced in this work. The statistical segment lengths b_{ref}, normalized to a common reference volume $v_{ref} = 118$ Å^3, were estimated from the plateau moduli G_N. The plateau moduli were determined from oscillatory shear rheology and van Gurp-Palmen analysis (**Figure S23**), as described in the Supporting Information. b_{ref} and G_N values for all blocks are provided in **Table 3**. For PN2M-*b*-PN2B and PN2M-*b*-PN1D, the conformational asymmetry is modest ($\varepsilon =$

1.3). In comparison, in PN2M-*b*-PN2D, the longer branches and higher grafting density amplify the conformational asymmetry ($\varepsilon = 1.9$).

Table 3. Plateau moduli (G_N) were determined by oscillatory shear rheology at temperatures T and used to estimate statistical segment lengths (b_{ref}). b_{ref} values are normalized to a common reference volume, 118 Å^3. Additional discussion of b_{ref} can be found in the Supporting Information.

Polymer	G_N (kPa)	T (°C)	b_{ref} (Å)
PN2M	460	120	5.84
PN2B	140	25	5.01
PN1D	165	110	5.06
PN2D	49	30	4.19

CONCLUSION

In this work, three series of block polymers were synthesized and studied in order to explore the impact of architectural asymmetry on Frank-Kasper phase formation in block polymer melts (**Figure 1**–**2**). Each diblock series featured the same core block, poly(norbornene *exo,exo*-dimethylester) (PN2M, R^1 = methyl), but a different coronal block: either (**A**) poly(norbornene *exo,exo*-di-*n*-butylester) (PN2B, R^2 = *n*-butyl); (**B**) poly(norbornene *exo*-*n*-decylimide) (PN1D, R^2 = *n*-decyl); or (**C**) poly(norbornene *exo,exo*-di-*n*-decylester) (PN2D, R^2 = *n*-decyl) (**Figure 3**). Manipulating the block polymer architecture tunes the way in which the coronal chains fill space and thereby influence symmetry selection.

PN2M-*b*-PN2D block polymers feature high self-concentration (**Table 2**) and high conformational asymmetry (**Table 3**) compared to PN2M-*b*-PN2B and PN2M-*b*-PN1D. The data suggest that only PN2D is a bottlebrush polymer, despite initial considerations that suggest all coronal blocks (PN2B, PN1D, and PN2D) experience significant steric crowding (**Table 1**). The bottlebrush architecture amplifies self-concentration and conformational asymmetry, opening the

window to complex low-symmetry phases. PN2M-*b*-PN2B and PN2M-*b*-PN1D access only the canonical diblock polymer morphologies, including body-centered cubic (BCC) spheres and hexagonally packed cylinders (HEX_C) (**Figure 4**). In contrast, the phase behavior of PN2M-*b*-PN2D reveals remarkable complexity (**Figure 5**): PN2M-*b*-PN2D block polymers can form Frank-Kasper σ and A15 phases (**Figure 6**) *via* nucleation and growth from dodecagonal quasicrystalline (DDQC) structures (**Figure 7**). Collectively, this work provides insight into the impact of molecular architecture on the formation of complex low-symmetry phases, expanding opportunities for molecular and materials design. Future work will expand this understanding, with particular focus on (1) scaling up bottlebrush dimensions and self-assembled length scales and (2) connecting recent theoretical predictions of bottlebrush chain statistics to the concepts of self-concentration and conformational asymmetry.

MATERIALS AND METHODS

Synthesis. The norbornene *exo,exo*-diester monomers (norbornene *exo,exo*-dimethylester, N2M; norbornene *exo,exo*-di-*n*-butylester, N2B; norbornene *exo,exo*-di-*n*-decylester, N2D) and norbornene *exo*-*n*-decylimide monomer (N1D) were synthesized according to a reported procedure.[61] Diblock polymers were synthesized by the sequential living ring-opening metathesis polymerization (ROMP) of norbornenyl monomers, mediated by the third-generation Grubbs metathesis catalyst, $[(H_2IMes)(pyr)_2(Cl)_2Ru{=}CHPh]$ (**G3**). Stock solutions of the monomers and catalyst were used to facilitate fine variations in block lengths. The degree of polymerization of each block was determined by the number of molar equivalents of each monomer relative to 1 equivalent of the **G3** catalyst. The volume fraction of was determined by the molar equivalents of the first monomer relative to the second monomer. Further discussion of monomer and block

polymer synthesis is provided in the Supporting Information. NMR, SEC, and DSC data are provided in **Figs. S1–S13**.

Instrumentation: SEC, DSC, SAXS/MAXS/WAXS, Rheology

Size-exclusion chromatography (SEC) data were obtained in THF using two Agilent PLgel MIXED-B 300 × 7.5 mm columns with 10 μm beads, connected to an Agilent 1260 Series pump, Wyatt 18-angle DAWN HELEOS light scattering detector, and Wyatt Optilab differential refractive index detector. Online determination of d*n*/d*c* assumed 100% mass elution under the peak of interest. Differential scanning calorimetry (DSC) measurements were performed on an TA Q1000 under a dry nitrogen atmosphere. The samples were heated to 150 °C at 10 °C/min to erase the thermal history, then cooled to −100 °C at 10 °C/min. Small-angle X-ray scattering (SAXS) data were collected at Beamline 12-ID-B of the Advanced Photon Source (APS) at Argonne National Laboratory. Mid- and wide-angle scattering (MAXS/WAXS) data were collected at the DuPont-Northwestern-Dow Collaborative Access Team (DND-CAT) Beamline, located at Sector 5 of the APS. The raw data were reduced and indexed using MATLAB software written by Dr. Byeongdu Lee (APS). Rheology data were collected on a Rheometric Scientific ARES rheometer using either 8 mm parallel plates (PN2M) or 25 mm parallel plates (PN2B, PN1D, PN2D). Strain sweeps were performed in order to identify the linear viscoelastic regime. Applied strains were between 1 and 10% for all samples. Frequency sweeps were performed in the linear viscoelastic regime. Further description of all instrumentation is provided in the Supporting Information.

ASSOCIATED CONTENT

Supporting Information. The Supporting Information is available free of charge on the ACS Publications website.

Experimental details, NMR spectra, representative SEC traces, compiled molecular characterization data and assigned morphologies, DSC thermograms, additional SAXS/WAXS/MAXS data, van Gurp-Palmen plots for homopolymers.

AUTHOR INFORMATION

Corresponding Authors

*Email: achang@umn.edu, bates001@umn.edu

The authors declare no competing financial interest.

ACKNOWLEDGMENT

This work was supported by the National Science Foundation under Grant DMR-1801993. A.B.C. thanks the Arnold O. Beckman Foundation for support through the Beckman Postdoctoral Fellowship. This work used the resources of the Advanced Photon Source (APS), a U.S. Department of Energy Office of Science User Facility operated by Argonne National Laboratory under Contract DE-AC02-06CH11357. SAXS, MAXS, and WAXS data were collected either at Beamline 12-ID-B of the APS or at the DuPont-Northwestern-Dow Collaborative Access Team (DND-CAT) Beamline, located at Sector 5 of the APS. The authors thank A. Lindsay, A. Mueller, and A. Jayaraman for assistance with select X-ray scattering measurements and for helpful discussions. The authors also gratefully acknowledge B. Lee, K. Dorfman, and M. Mahanthappa for helpful discussions.

REFERENCES

(1) Whitesides, G. M.; Grzybowski, B. Self-Assembly at All Scales. *Science* **2002**, *295*, 2418–2421.

(2) Ziherl, P.; Kamien, R. D. Maximizing Entropy by Minimizing Area: Towards a New Principle of Self-Organization. *J. Phys. Chem. B* **2001**, *105*, 10147–10158.

(3) Israelachvili, J. N.; Mitchell, D. J.; Ninham, B. W. Theory of Self-Assembly of Hydrocarbon Amphiphiles into Micelles and Bilayers. *J. Chem. Soc., Faraday Trans. 2* **1976**, *72*, 1525–1568.

(4) Frank, F. C.; Kasper, J. S. Complex Alloy Structures Regarded as Sphere Packings. II. Analysis and Classification of Representative Structures. *Acta Crystallogr.* **1959**, *12*, 483–499.

(5) Shoemaker, D. P.; Shoemaker, C. B. Concerning the Relative Numbers of Atomic Coordination Types in Tetrahedrally Close Packed Metal Structures. *Acta Crystallogr. B* **1986**, *42*, 3–11.

(6) Balagurusamy, V. S. K.; Ungar, G.; Percec, V.; Johansson, G. Rational Design of the First Spherical Supramolecular Dendrimers Self-Organized in a Novel Thermotropic Cubic Liquid-Crystalline Phase and the Determination of Their Shape by X-ray Analysis. *J. Am. Chem. Soc.* **1997**, *119*, 1539–1555.

(7) Hudson, S. D.; Jung, H.-T.; Percec, V.; Cho, W.-D.; Johansson, G.; Ungar, G.; Balagurusamy, V. S. K. Direct Visualization of Individual Cylindrical and Spherical Supramolecular Dendrimers. *Science* **1997**, *278*, 449–452.

(8) Ungar, G.; Liu, Y.; Zeng, X.; Percec, V.; Cho, W.-D. Giant Supramolecular Liquid Crystal Lattice. *Science* **2003**, *299*, 1208–1211.

(9) Cho, B.-K.; Jain, A.; Gruner, S. M.; Wiesner, U. Mesophase Structure-Mechanical and Ionic Transport Correlations in Extended Amphiphilic Dendrons. *Science* **2004**, *305*, 1598–1601.

(10) Vargas, R.; Mariani, P.; Gulik, A.; Luzzati, V. Cubic Phases of Lipid-Containing Systems: The Structure of Phase Q223 (Space Group Pm3n). An X-Ray Scattering Study. *J. Mol. Biol.* **1992**, *225*, 137–145.

(11) Seddon, J. M.; Zeb, N.; Templer, R. H.; McElhaney, R. N.; Mannock, D. A. An Fd3m Lyotropic Cubic Phase in a Binary Glycolipid/Water System. *Langmuir* **1996**, *12*, 5250–5253.

(12) Sakya, P.; Seddon, J. M.; Templer, R. H.; Mirkin, R. J.; Tiddy, G. J. T. Micellar Cubic Phases and Their Structural Relationships: The Nonionic Surfactant System $C_{12}EO_{12}$/Water. *Langmuir* **1997**, *13*, 3706–3714.

(13) Sakamoto, Y.; Kaneda, M.; Terasaki, O.; Zhao, D. Y.; Kim, J. M.; Stucky, G.; Shin, H. J.; Ryoo, R. Direct Imaging of the Pores and Cages of Three-Dimensional Mesoporous Materials. *Nature* **2000**, *408*, 449–453.

(14) Kim, S. A.; Jeong, K.-J.; Yethiraj, A.; Mahanthappa, M. K. Low-Symmetry Sphere Packings of Simple Surfactant Micelles Induced by Ionic Sphericity. *Proc. Natl. Acad. Sci.* **2017**, *114*, 4072–4077.

(15) Huang, M.; Hsu, C.-H.; Wang, J.; Mei, S.; Dong, X.; Li, Y.; Li, M.; Liu, H.; Zhang, W.; Aida, T.; Zhang, W.-B.; Yue, K.; Cheng, S. Z. D. Selective Assemblies of Giant Tetrahedra *via* Precisely Controlled Positional Interactions. *Science* **2015**, *348*, 424–428.

(16) Yue, K.; Huang, M.; Marson, R. L.; He, J.; Huang, J.; Zhou, Z.; Wang, J.; Liu, C.; Yan, X.; Wu, K.; Guo, Z.; Liu, H.; Zhang, W.; Ni, P.; Wesdemiotis, C.; Zhang, W.-B.; Glotzer, S.

C.; Cheng, S. Z. D. Geometry Induced Sequence of Nanoscale Frank–Kasper and Quasicrystal Mesophases in Giant Surfactants. *Proc. Natl. Acad. Sci.* **2016**, *113*, 14195–14200.
(17) Su, Z.; Hsu, C.-H.; Gong, Z.; Feng, X.; Huang, J.; Zhang, R.; Wang, Y.; Mao, J.; Wesdemiotis, C.; Li, T.; Seifert, S.; Zhang, W.; Aida, T.; Huang, M.; Cheng, S. Z. D. Identification of a Frank–Kasper Z Phase from Shape Amphiphile Self-Assembly. *Nat. Chem.* **2019**, *11*, 899–905.
(18) Lee, S.; Bluemle, M. J.; Bates, F. S. Discovery of a Frank-Kasper σ Phase in Sphere-Forming Block Copolymer Melts. *Science* **2010**, *330*, 349–353.
(19) Bates, M. W.; Lequieu, J.; Barbon, S. M.; Lewis, R. M.; Delaney, K. T.; Anastasaki, A.; Hawker, C. J.; Fredrickson, G. H.; Bates, C. M. Stability of the A15 phase in Diblock Copolymer Melts. *Proc. Natl. Acad. Sci.* **2019**, *116*, 13194–13199.
(20) Lee, S.; Leighton, C.; Bates, F. S. Sphericity and symmetry Breaking in the Formation of Frank–Kasper Phases from One Component Materials. *Proc. Natl. Acad. Sci.* **2014**, *111*, 17723–17731.
(21) Gillard, T. M.; Lee, S.; Bates, F. S. Dodecagonal Quasicrystalline Order in a Diblock Copolymer Melt. *Proc. Natl. Acad. Sci.* **2016**, *113*, 5167–5172.
(22) Kim, K.; Schulze, M. W.; Arora, A.; Lewis, R. M.; Hillmyer, M. A.; Dorfman, K. D.; Bates, F. S. Thermal Processing of Diblock Copolymer Melts Mimics Metallurgy. *Science* **2017**, *356*, 520–523.
(23) Schulze, M. W.; Lewis, R. M.; Lettow, J. H.; Hickey, R. J.; Gillard, T. M.; Hillmyer, M. A.; Bates, F. S. Conformational Asymmetry and Quasicrystal Approximants in Linear Diblock Copolymers. *Phys. Rev. Lett.* **2017**, *118*, 207801.
(24) Kim, K.; Arora, A.; Lewis, R. M.; Liu, M.; Li, W.; Shi, A.-C.; Dorfman, K. D.; Bates, F. S. Origins of low-Symmetry Phases in Asymmetric Diblock Copolymer Melts. *Proc. Natl. Acad. Sci.* **2018**, *115*, 847–854.
(25) Jeon, S.; Jun, T.; Jo, S.; Ahn, H.; Lee, S.; Lee, B.; Ryu, D. Y. Frank–Kasper Phases Identified in PDMS-b-PTFEA Copolymers with High Conformational Asymmetry. *Macromol. Rapid Commun.* **2019**, *40*, 1900259.
(26) Chanpuriya, S.; Kim, K.; Zhang, J.; Lee, S.; Arora, A.; Dorfman, K. D.; Delaney, K. T.; Fredrickson, G. H.; Bates, F. S. Cornucopia of Nanoscale Ordered Phases in Sphere-Forming Tetrablock Terpolymers. *ACS Nano* **2016**, *10*, 4961–4972.
(27) Zhang, J.; Bates, F. S. Dodecagonal Quasicrystalline Morphology in a Poly(styrene-b-isoprene-b-styrene-b-ethylene oxide) Tetrablock Terpolymer. *J. Am. Chem. Soc.* **2012**, *134*, 7636–7639.
(28) Flory, P. J. *Principles of Polymer Chemistry*; Cornell University Press: Ithaca, NY, 1953.
(29) de Gennes, P.-G. *Scaling Concepts in Polymer Physics*; Cornell University Press: Ithaca, NY, 1979.
(30) Fredrickson, G. H. *The Equilibrium Theory of Inhomogeneous Polymers*; Oxford University Press: New York, 2006.
(31) Lewis, R. M.; Arora, A.; Beech, H. K.; Lee, B.; Lindsay, A. P.; Lodge, T. P.; Dorfman, K. D.; Bates, F. S. Role of Chain Length in the Formation of Frank-Kasper Phases in Diblock Copolymers. *Phys. Rev. Lett.* **2018**, *121*, 208002.
(32) Xie, N.; Li, W.; Qiu, F.; Shi, A.-C. σ Phase Formed in Conformationally Asymmetric AB-Type Block Copolymers. *ACS Macro Lett.* **2014**, *3*, 906–910.

(33) Ungar, G.; Zeng, X. Frank–Kasper, Quasicrystalline and Related Phases in Liquid Crystals. *Soft Matter* **2005**, *1*, 95–106.
(34) Huang, N.; Imam, M. R.; Sienkowska, M. J.; Peterca, M.; Holerca, M. N.; Wilson, D. A.; Rosen, B. M.; Partridge, B. E.; Xiao, Q.; Percec, V. Supramolecular Spheres Assembled from Covalent and Supramolecular Dendritic Crowns Dictate the Supramolecular Orientational Memory Effect Mediated by Frank–Kasper Phases. *Giant* **2020**, *1*, 100001.
(35) Perroni, D. V.; Mahanthappa, M. K. Inverse Pm3n Cubic Micellar Lyotropic Phases from Zwitterionic Triazolium Gemini Surfactants. *Soft Matter* **2013**, *9*, 7919–7922.
(36) Feng, X.; Zhang, R.; Li, Y.; Hong, Y.-l.; Guo, D.; Lang, K.; Wu, K.-Y.; Huang, M.; Mao, J.; Wesdemiotis, C.; Nishiyama, Y.; Zhang, W.; Zhang, W.; Miyoshi, T.; Li, T.; Cheng, S. Z. D. Hierarchical Self-Organization of ABn Dendron-like Molecules into a Supramolecular Lattice Sequence. *ACS Cent. Sci.* **2017**, *3*, 860–867.
(37) Gao, Y.; Deng, H.; Li, W.; Qiu, F.; Shi, A.-C. Formation of Nonclassical Ordered Phases of AB-Type Multiarm Block Copolymers. *Phys. Rev. Lett.* **2016**, *116*, 068304.
(38) Qiang, Y.; Li, W.; Shi, A.-C. Stabilizing Phases of Block Copolymers with Gigantic Spheres *via* Designed Chain Architectures. *ACS Macro Lett.* **2020**, 668–673.
(39) Daniel, W. F. M.; Burdynska, J.; Vatankhah-Varnoosfaderani, M.; Matyjaszewski, K.; Paturej, J.; Rubinstein, M.; Dobrynin, A. V.; Sheiko, S. S. Solvent-Free, Supersoft and Superelastic Bottlebrush Melts and Networks. *Nat. Mater.* **2016**, *15*, 183–189.
(40) Liang, H.; Cao, Z.; Wang, Z.; Sheiko, S. S.; Dobrynin, A. V. Combs and Bottlebrushes in a Melt. *Macromolecules* **2017**, *50*, 3430–3437.
(41) Reddy, A.; Buckley, M. B.; Arora, A.; Bates, F. S.; Dorfman, K. D.; Grason, G. M. Stable Frank–Kasper phases of Self-Assembled, Soft Matter Spheres. *Proc. Natl. Acad. Sci.* **2018**, *115*, 10233–10238.
(42) Elli, S.; Ganazzoli, F.; Timoshenko, E. G.; Kuznetsov, Y. A.; Connolly, R. Size and Persistence Length of Molecular Bottle-Brushes by Monte Carlo Simulations. *J. Chem. Phys.* **2004**, *120*, 6257–6267.
(43) Paturej, J.; Sheiko, S. S.; Panyukov, S.; Rubinstein, M. Molecular Structure of Bottlebrush Polymers in Melts. *Sci. Adv.* **2016**, *2*, e1601478.
(44) López-Barrón, C. R.; Brant, P.; Eberle, A. P. R.; Crowther, D. J. Linear Rheology and Structure of Molecular Bottlebrushes with Short Side Chains. *J. Rheol.* **2015**, *59*, 865–883.
(45) López-Barrón, C. R.; Tsou, A. H.; Hagadorn, J. R.; Throckmorton, J. A. Highly Entangled α-Olefin Molecular Bottlebrushes: Melt Structure, Linear Rheology, and Interchain Friction Mechanism. *Macromolecules* **2018**, *51*, 6958–6966.
(46) Ediger, M. D.; Angell, C. A.; Nagel, S. R. Supercooled Liquids and Glasses. *J. Phys. Chem.* **1996**, *100*, 13200–13212.
(47) Debenedetti, P. G.; Stillinger, F. H. Supercooled Liquids and the Glass Transition. *Nature* **2001**, *410*, 259–267.
(48) Yamamoto, A. Crystallography of Quasiperiodic Crystals. *Acta Crystallogr. A* **1996**, *52*, 509–560.
(49) Iwami, S.; Ishimasa, T. Dodecagonal Quasicrystal in Mn-Based Quaternary Alloys Containing Cr, Ni and Si. *Philos. Mag. Lett.* **2015**, *95*, 229–236.
(50) Holerca, M. N.; Sahoo, D.; Partridge, B. E.; Peterca, M.; Zeng, X.; Ungar, G.; Percec, V. Dendronized Poly(2-oxazoline) Displays within only Five Monomer Repeat Units Liquid Quasicrystal, A15 and σ Frank–Kasper Phases. *J. Am. Chem. Soc.* **2018**, *140*, 16941–16947.

(51) Peterca, M.; Imam, M. R.; Hudson, S. D.; Partridge, B. E.; Sahoo, D.; Heiney, P. A.; Klein, M. L.; Percec, V. Complex Arrangement of Orthogonal Nanoscale Columns *via* a Supramolecular Orientational Memory Effect. *ACS Nano* **2016**, *10*, 10480–10488.
(52) Jayaraman, A.; Zhang, D. Y.; Dewing, B. L.; Mahanthappa, M. K. Path-Dependent Preparation of Complex Micelle Packings of a Hydrated Diblock Oligomer. *ACS Cent. Sci.* **2019**, *5*, 619–628.
(53) Lindsay, A. P.; Lewis, R. M.; Lee, B.; Peterson, A. J.; Lodge, T. P.; Bates, F. S. A15, σ, and a Quasicrystal: Access to Complex Particle Packings *via* Bidisperse Diblock Copolymer Blends. *ACS Macro Lett.* **2020**, *9*, 197–203.
(54) Lachmayr, K. K.; Wentz, C. M.; Sita, L. R. An Exceptionally Stable and Scalable Sugar–Polyolefin Frank–Kasper A15 Phase. *Angew. Chem. Int. Ed.* **2020**, *59*, 1521–1526.
(55) Zeng, X.; Ungar, G.; Liu, Y.; Percec, V.; Dulcey, A. E.; Hobbs, J. K. Supramolecular Dendritic Liquid Quasicrystals. *Nature* **2004**, *428*, 157–160.
(56) López-Barrón, C. R.; Tsou, A. H.; Younker, J. M.; Norman, A. I.; Schaefer, J. J.; Hagadorn, J. R.; Throckmorton, J. A. Microstructure of Crystallizable α-Olefin Molecular Bottlebrushes: Isotactic and Atactic Poly(1-octadecene). *Macromolecules* **2018**, *51*, 872–883.
(57) López-Barrón, C. R.; Shivokhin, M. E.; Hagadorn, J. R. Extensional Rheology of Highly-Entangled α-Olefin Molecular Bottlebrushes. *J. Rheol.* **2019**, *63*, 917–926.
(58) Tanford, C. Micelle Shape and Size. *J. Phys. Chem.* **1972**, *76*, 3020–3024.
(59) Zinn, T.; Willner, L.; Lund, R.; Pipich, V.; Appavou, M.-S.; Richter, D. Surfactant or Block Copolymer Micelles? Structural Properties of a Series of Well-Defined n-Alkyl–PEO Micelles in Water Studied by SANS. *Soft Matter* **2014**, *10*, 5212–5220.
(60) Jones, A. T. Crystallinity in Isotactic Polyolefins with Unbranched Side Chains. *Makromol. Chem.* **1964**, *71*, 1–32.
(61) Chang, A. B.; Lin, T.-P.; Thompson, N. B.; Luo, S.-X.; Liberman-Martin, A. L.; Chen, H.-Y.; Lee, B.; Grubbs, R. H. Design, Synthesis, and Self-Assembly of Polymers with Tailored Graft Distributions. *J. Am. Chem. Soc.* **2017**, *139*, 17683–17693.

For Table of Contents (TOC) Only: